ln $[CF_3]$ versus injector position x, the pseudo-first-order reaction rate constant, $k_1 = k_b[\text{Atoms}]$, is obtained from the slope according to

$$k_1 = k_w\left(\frac{a}{b}\right) - v\left\{\frac{\mathrm{d}\ \ln\ [CF_3]_t}{\mathrm{d}x}\right\}_{\text{expt}} \tag{11}$$

Appendix B

A modified rate equation is derived to account for the observed linear decrease in the atomic reactant concentration along the reaction zone that accompanied the use of C_2F_6 as the CF_3 radical precursor (see text). In this case the rate equation for CF_3 decay can be written

$$-v\frac{\mathrm{d}[CF_3]}{[CF_3]} = k_b[O]_x\,\mathrm{d}x + k_w\,\mathrm{d}x \tag{12}$$

where x is distance measured along the reaction zone starting from the sampling aperture, $[O]_x$ is the concentration of atoms as a function of distance x, v is the linear flow velocity, and k_w is the first-order rate constant for wall loss of CF_3 radicals in the reaction zone. Integrating the equation between the initial, observed reaction time, $t_1 = x_1/v$, and some arbitrary time t between t_1 and the final reaction time, $t_2 = x_2/v$, yields

$$-v\ln\left\{\frac{[CF_3]_x}{[CF_3]_{x_1}}\right\} = k_b\int_{x_1}^{x}[O]_x\,\mathrm{d}x + k_w(x - x_1) \tag{13}$$

$[O]_x$ was found empirically to be linear in x as expressed in

$$[O]_x = [O]_{x_1} - \frac{[O]_{x_1} - [O]_{x_2}}{x_2 - x_1}(x - x_1) = [O]_{x_1} - \Delta(x - x_1) \tag{14}$$

where Δ is the measured slope of the atomic reactant profile. Substitution for $[O]_x$ in eq 12 and integration leads, after rearrangement, to

$$-v\ln\left\{\frac{[CF_3]_x}{[CF_3]_{x_1}}\right\} = \left(\frac{-k_b\Delta}{2}\right)x^2 + (k_b[O]_{x_1} + k_b\Delta x_1 + k_w)x + \left(-k_bx_1 - \frac{\Delta x_1^2}{2} - k_wx_1\right) \tag{15}$$

or

$$\ln\left\{\frac{[CF_3]_x}{[CF_3]_{x_1}}\right\} = Ax^2 + Bx + C \tag{16}$$

where

$$A = \frac{k_b\Delta}{2v}$$

$$B = \frac{-k_b[O]_{x_1} - k_b\Delta x_1 - k_w}{v}$$

$$C = \frac{k_bx_1 + (\Delta x_1^2/2) + k_wx_1}{v}$$

Registry No. CF_3, 2264-21-3; O, 17778-80-2; N, 17778-88-0.

High-Temperature Photochemistry Kinetics Studies of the Reactions of H(1^2S) and D(1^2S) with N_2O

Paul Marshall, Taeho Ko, and Arthur Fontijn*

High-Temperature Reaction Kinetics Laboratory, Department of Chemical Engineering, Rensselaer Polytechnic Institute, Troy, New York 12180-3590 *(Received: June 16, 1988)*

The H + N_2O (1) and D + N_2O (2) reactions have been investigated by using the high-temperature photochemistry (HTP) technique. Empirical fits to the pressure-independent rate coefficients yield $k_1(T) = 4.2 \times 10^{-14}\exp(-2290\ \text{K}/T) + 3.7 \times 10^{-10}\exp(-8430\ \text{K}/T)$ and $k_2(T) = 3.5 \times 10^{-13}\exp(-3600\ \text{K}/T) + 5.3 \times 10^{-10}\exp(-9170\ \text{K}/T)$ cm^3 molecule^{-1} s^{-1} over the ranges 410-1230 and 450-1210 K, respectively. The 2σ precision of these results is better than 11% and the 95% accuracy limits are assessed at about ±25%. The kinetic isotope effect $x(T) = k_1(T)/k_2(T)$ decreases from 2.2 at 450 K to 1.3 at 1200 K, behavior contrary to classical transition-state theory which predicts $x(T)$ increasing with temperature. The data are qualitatively consistent with a rate-controlling step that is dominated by tunneling at the lower end of the temperature range.

1. Introduction

Rate coefficient measurements using the HTP technique have previously been reported[1] for the reaction

$$H + N_2O \rightarrow OH + N_2 \tag{1}$$

Ab initio quantum calculations suggested that the rate determining step is isomerization of an HNNO intermediate, leading to N_2 and OH as major products. Non-Arrhenius behavior of the measured $k_1(T)$ was interpreted in terms of quantum-mechanical tunneling during the intramolecular transfer of H atoms from N to O via a cyclic $\overline{\text{HNNO}}^{\ddagger}$ transition state.

In order to further examine this hypothesis we have made kinetic measurements on the deuterium analogue reaction

$$D + N_2O \rightarrow OD + N_2 \tag{2}$$

for which no previous experimental data are available. To provide the most reliable comparison with $k_1(T)$, determinations of k_2 were interlaced with redeterminations of k_1. The temperature dependence of the kinetic isotope effect is discussed in the context of different reaction mechanisms.

2. Experimental Technique

The HTP reactor used has been described.[2] Briefly, H or D atoms are generated by flash photolysis of NH_3 or ND_3, respectively, through a Suprasil quartz lens ($\lambda > 160$ nm). The relative H and D concentrations are monitored by time-resolved, atomic-resonance fluorescence spectroscopy with pulse counting

(1) Marshall, P.; Fontijn, A. *J. Chem. Phys.* **1987**, *86*, 5540.

(2) Marshall, P.; Fontijn, A. *J. Chem. Phys.* **1986**, *85*, 2637.

0022-3654/89/2093-1922$01.50/0

and signal averaging. The resonance radiation for the electronic transitions [H(2^2P)–H(1^2S), λ = 121.6 nm] or [D(2^2P)–D(1^2S), λ = 121.5 nm] is provided by a microwave discharge through 1.5 Torr of 1% H_2 or D_2 in He. These gases are Linde Custom Grade. The resulting fluorescence signal is spectrally isolated by a dry-air filter (2.5 cm path length; atmospheric pressure) in front of the photomultiplier tube (PMT). The reaction zone is defined by the intersection of the field of view of the PMT and the cones of light from the flash lamp and resonance lamp.

The N_2O and NH_3 or ND_3 with about 1% of total Ar flow are injected into the reactor through the movable cooled inlet, while the remainder of the Ar enters the reactor through the upstream (bottom) side, 47 cm from the reaction observation zone. In the earlier study[1] the 0.6 cm diameter mouth of the cooled inlet was capped with an inverted alumina cup, 2.5 cm diameter, with eight 0.2 cm diameter side holes to assure good mixing. In the present work this cap was not used except for checks (see below). It follows that careful attention must be paid to mixing because [N_2O] is calculated under the assumption of complete dispersion. Setting as a minimum condition that the radial concentration gradient in the observed reaction zone be <5% of the initial gradient, we calculate that the diffusion time required for 95% reduction in the radial [N_2O] gradient is given by[3] $t_{95\%} = 0.052d^2/D_{AB}$, where d is the diameter of the reaction tube, 5.1 cm, and D_{AB} is the diffusion coefficient[4] between N_2O and Ar. Actual mixing will be faster since turbulence at the inlet will accelerate mixing, and the inlet is not an exact point source. The mean residence time of reactant gases is given by $t = z/\bar{v}$, where z is the inlet-to-reaction zone distance and $\bar{v}$ is the average linear gas velocity. Eight measurements of k_1 at 770 K and 160 Torr showed that the average of the four measurements for $t < t_{95\%}$ was larger by about 30% than the average of the four measurements for $t > t_{95\%}$, while k_1 for $t > t_{95\%}$ agreed with k_1 for N_2O premixed with the bath gas; i.e., t is essentially infinite. Below 650 K, k_1 for $t > t_{95\%}$ also agreed with those obtained when the reactant gases were injected through the alumina cap. Above 650 K, the use of the cap led to consistently lower rate coefficients which we believe is due to partial decomposition of the reactant gases.

The reaction gases used were Linde 99.99% Anhydrous Grade Ar; Matheson 99.99% Ultra High Purity N_2O; Matheson 99.998% Semiconductor Purity NH_3; and Cambridge Isotope Laboratories 99.5% isotopic purity ND_3, all directly from the cylinder. For some of the rate coefficient measurements at temperatures below about 850 K, N_2O was further purified by three freeze–pump–thaw cycles using liquid nitrogen, and fed from a storage bulb.

The decrease in [H] in experiments to study reaction 1 was due to the reactions with N_2O and NH_3, and diffusion out of the reaction zone. Under the pseudo-first-order conditions used, [H] ≪ [N_2O], [NH_3]

$$-\mathrm{d[H]}/\mathrm{d}t = k_1[\mathrm{H}][\mathrm{N_2O}] + k_3[\mathrm{H}][\mathrm{NH_3}] + k_{\mathrm{diff}}[\mathrm{H}] \quad (3)$$

$$= k_{\mathrm{ps1}}[\mathrm{H}] \quad (4)$$

The slope of a plot of k_{ps1}, at constant [NH_3], versus [N_2O] yielded k_1; equations for k_2 are analogous to those for k_1. Typically six values of [N_2O] from zero to $[N_2O]_{max}$ (see Tables I and II) were used for each determination of k_1 or k_2. k_{ps1} was obtained by fitting[5] the observed emission intensities I to

$$I = I_0 \exp(-k_{\mathrm{ps1}}t) + B \quad (5)$$

where I_0 is the fluorescence intensity at $t = 0$ and B is the steady background from scattered light. To check the linearity of the fluorescence intensity with atom concentration, $[H]_{t=0}$ and $[D]_{t=0}$ were varied in separate room temperature experiments by changing the energy, F, dissipated in the flash lamp at given [NH_3] and [ND_3], respectively.[6] Linear plots of I_0 versus F were obtained.

3. Experimental Results

The 53 measurements of k_1 in the 410–1230 K range and the 54 measurements of k_2 in the 450–1210 K range are summarized in Tables I and II, respectively. Also given there are the experimental parameters: total pressure, P; total concentration, [M]; $\bar{v}$; z; F; and [NH_3] or [ND_3]. In typical $1000/T = 0.5$ K^{-1} intervals, these parameters were varied by factors of about 5. Within the experimental scatter there is no consistent dependence of k_1 or k_2 on any of these parameters. These variations in F, [NH_3], and [ND_3] imply that $[H]_{t=0}$ and $[D]_{t=0}$ were accordingly changed by an order of magnitude; the mean residence time, $z/\bar{v}$, was varied similarly by an order of magnitude. The independence of these atom concentrations shows that kinetic complications from reaction products or photolytic fragments were negligible. In addition, the independence from $z/\bar{v}$ demonstrates that the gases were well-mixed, that thermal equilibrium was achieved, and that heterogeneous decomposition within the reactor was not significant. For k_1, the results obtained with and without N_2O purification were consistent. However, the results for the slower reaction 2 were influenced by impurities; specifically, those k_2 without N_2O purification were consistently larger by a factor of about 1.7 at $T < 570$ K.

To fit the present data, two expressions were considered

$$k(T) = A(T/\mathrm{K})^n \exp(-B\ \mathrm{K}/T)\ \mathrm{cm^3\ molecule^{-1}\ s^{-1}}$$

$$k(T) = A \exp(-B\ \mathrm{K}/T) + C \exp(-D\ \mathrm{K}/T)\ \mathrm{cm^3\ molecule^{-1}\ s^{-1}}$$

Although both give similarly good fits, the former equation gives parameters that are difficult to support theoretically: $A = 3.9 \times 10^{-53}$, $n = 12.6$, and $B = -3520$ for $k_1(T)$; and $A = 3.0 \times 10^{-44}$, $n = 9.9$, and $B = -1390$ for $k_2(T)$. The latter expression yields the nonlinear, least-squares fits:

$$k_1(T) = 4.2 \times 10^{-14} \exp(-2290\ \mathrm{K}/T) + 3.7 \times 10^{-10} \exp(-8430\ \mathrm{K}/T)\ \mathrm{cm^3\ molecule^{-1}\ s^{-1}} \quad (6)$$

$$k_2(T) = 3.5 \times 10^{-13} \exp(-3600\ \mathrm{K}/T) + 5.3 \times 10^{-10} \exp(-9170\ \mathrm{K}/T)\ \mathrm{cm^3\ molecule^{-1}\ s^{-1}} \quad (7)$$

The variances[7,8] for the parameters A, B, C, and D, are as follows: for $k_1(T)$, $\sigma_A^2 = 6.8 \times 10^{-31}$, $\sigma_B^2 = 2.6 \times 10^2$, $\sigma_C^2 = 1.7 \times 10^{-20}$, $\sigma_D^2 = 9.7 \times 10^4$; for $k_2(T)$, $\sigma_A^2 = 9.9 \times 10^{-31}$, $\sigma_B^2 = 2.0 \times 10^2$, $\sigma_C^2 = 3.8 \times 10^{-20}$, $\sigma_D^2 = 1.2 \times 10^5$; the associated covariances are as follows: for $k_1(T)$, $\sigma_{AB} = -9.8 \times 10^{-17}$, $\sigma_{AC} = -1.6 \times 10^{-26}$, $\sigma_{AD} = -4.2 \times 10^{-14}$, $\sigma_{BC} = 9.4 \times 10^{-11}$, $\sigma_{BD} = 2.3 \times 10^2$, $\sigma_{CD} = 4.0 \times 10^{-8}$; for $k_2(T)$, $\sigma_{AB} = -1.6 \times 10^{-16}$, $\sigma_{AC} = -2.4 \times 10^{-26}$, $\sigma_{AD} = -4.5 \times 10^{-14}$, $\sigma_{BC} = 2.3 \times 10^{-10}$, $\sigma_{BD} = 4.1 \times 10^2$, $\sigma_{CD} = 6.6 \times 10^{-8}$. Since the parameters A, B, C, and D are dependent, both the variances and covariances are taken into account in obtaining confidence intervals. The 2σ precision ranges from ±4% at 410 K to ±11% at 1230 K for $k_1(T)$ and from ±3% at 450 K to ±9% at 1210 K for $k_2(T)$. Then allowing, somewhat arbitrarily, about ±20% for possible systematic errors, 95% confidence intervals are about ±25%.

The envelope of measured k_1 obtained here overlaps with that of the previous HTP data set.[1] However, above 650 K there is

(3) Taylor, G. *Proc. R. Soc.* **1953**, *A219*, 186.

(4) Only the N_2O–Ar pair need be considered, because diffusion of the heavier N_2O is slower than that of NH_3 or ND_3. D_{AB} was obtained from the semiempirical relationship eq 16.3-1 of: Bird, R. B.; Stewart, W. E.; Lightfoot, E. N. *Transport Phenomena*; Wiley: New York, 1960; p 505.

(5) Marshall, P. *Comput. Chem.* **1987**, *11*, 219.

(6) Relative values of $[H]_{t=0}$ were obtained from relative values of the product F[NH_3]. Such experiments at any temperature would check whether the atom concentration was sufficiently low for fluorescence to be proportional to concentration, see e.g.: Husain, D.; Krause, L.; Slater, N. K. H. *J. Chem. Soc., Faraday Trans. 2* **1977**, *73*, 1678. For checks on the linearity of fluorescence with [H], the lowest T used, i.e., room temperature, is the most sensitive. There the broadening of the atomic absorption lines is smallest and hence any effects from line reversal in the resonance lamp or from mismatched line shapes between emitting and absorbing atoms are greatest. See e.g.: Fontijn, A.; Felder, W. In *Reactive Intermediates in the Gas Phase*; Setser, D. W., Ed.; Academic: New York, 1979; Chapter 2.

(7) Bevington, P. R. *Data Reduction and Error Analysis for the Physical Sciences*; McGraw-Hill: New York, 1969; p 242.

(8) Wentworth, W. E. *J. Chem. Educ.* **1965**, *42*, 96.

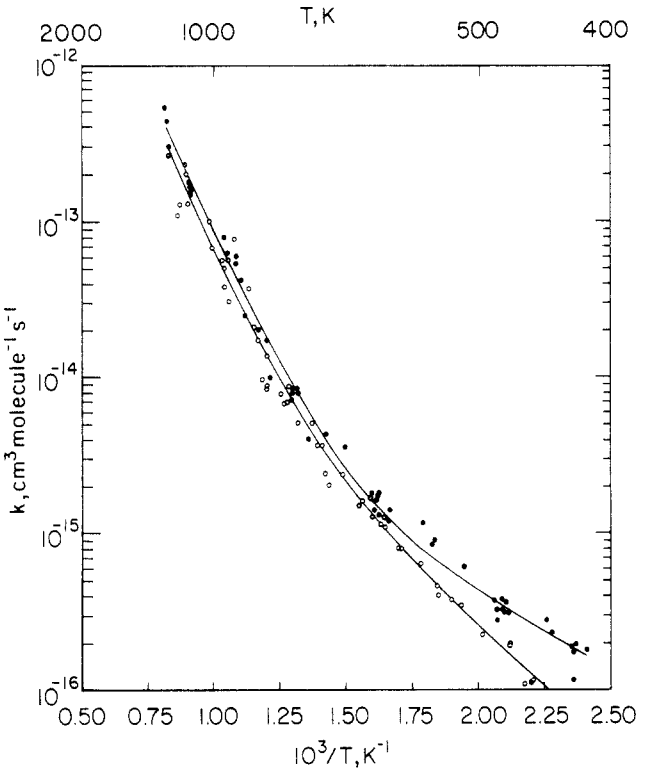

Figure 1. Plot of the rate coefficients obtained for the reactions of H (●) and D (○) with N_2O, showing the best fits.

a systematic difference between the fitted $k_1(T)$ expressions. In this temperature range the present $k_1(T)$ results are between factors of 1.4 and 1.8 greater than the earlier determinations.[1] Those were made by using the capped inlet (see section 2) at all temperatures. Putting the cap back reproduced the earlier HTP results.

The only other direct measurements of reaction 1 in the present temperature range were made with a discharge/fast-flow reactor by Albers et al.[9] Their fit lies below that of eq 6 by factors of 1.3–1.8 for 800 K < T < 1110 K. The present results agree to within the 1.6 uncertainty factors of the recommendation for T > 700 K of Hanson and Salimian,[10] based in part on that of Baulch et al.[11]

There are apparently no other measurements of k_2 to compare with the present data.

These data allow evaluation of the kinetic isotope effect $x(T) = k_1(T)/k_2(T)$. Figure 1 shows that x decreases as T increases and becomes approximately constant above 700 K. Figure 2 gives a plot of $x(T)$ vs T, evaluated from eq 6 and 7, and smoothed out by fitting to the form[12] $A \exp(-BT) + C$. The 95% confidence intervals for $x(T)$, derived by combining the intervals for each rate coefficient, are about ±35%.

4. Discussion

A theoretical study of reaction 1 by the BAC-MP4 method has previously been reported.[1] The approach is outlined in the Appendix. That work[1] discussed that a priori two distinct channels leading to OH and N_2 are possible. One is direct H-atom attack at the oxygen end of N_2O, the other, with a lower entrance barrier V_1, involves formation of an HNNO intermediate. The intermediate can decompose to final products via a 1,3-hydrogen shift, with an energy barrier V_2, through the NNOH configuration. The

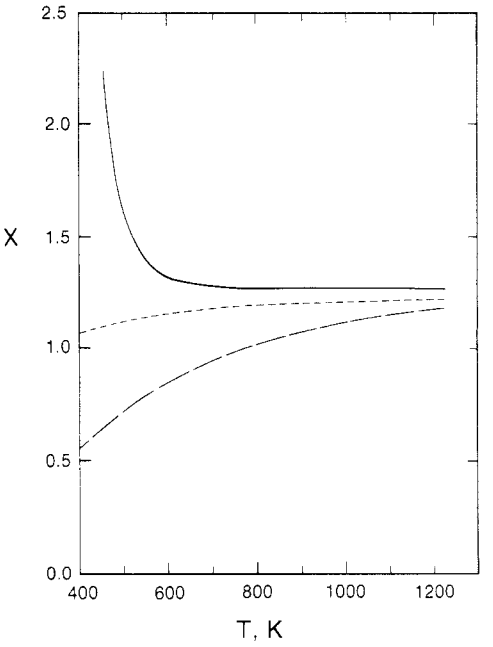

Figure 2. Comparison of the experimental kinetic isotope effect x for H + N_2O (—) to CTST calculations, without tunneling, for two transition states: NNOH‡ (- - -) and HNNO‡ (– – –).

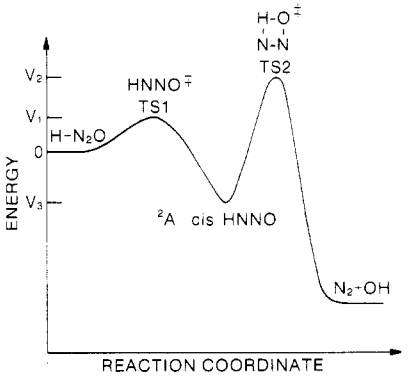

Figure 3. Schematic diagram of the vibrationally adiabatic ground-state pathway for H + N_2O, based on BAC-MP4 calculations, ref 14, *not to scale*.

one-dimensional reaction coordinate for the vibrationally adiabatic ground state of this pathway is shown schematically on Figure 3. The second mechanism is favored because transition-state theory calculations incorporating one-dimensional Eckart tunneling corrections give much closer agreement with the observed $k_1(T)$ for the second mechanism.[1] According to that simple treatment, the large degree of tunneling possible for the intramolecular H-atom transfer, where the energy barrier is narrow, slows the reduction of k_1 with decreasing temperature. This is consistent with the strongly curved Arrhenius plots of k_1 found earlier[1] and here (Figure 1).[13]

Here we extend consideration of the 1,3-H shift pathway, primarily to interpret the kinetic isotope effect $x(T)$ and also to further examine the pressure independence of both k_1 and k_2. The kinetics may be written in microcanonical form

$$H + N_2O \underset{k_{-a}(E)}{\overset{k_a(E)}{\rightleftharpoons}} HNNO^*(E) \xrightarrow{k_b(E)} OH + N_2 \qquad (8)$$

(9) Albers, E. A.; Hoyermann, K.; Schacke, H.; Schmatjko, K. J.; Wagner, H. Gg.; Wolfrum, J. *Symp. (Int.) Combust., [Proc.], 15th* **1975**, 765.

(10) Hanson, R. K.; Salimian, S. In *Combustion Chemistry*; Gardiner, W. C., Jr., Ed.; Springer: New York, 1984; p 404.

(11) Baulch, D. L.; Drysdale, D. D.; Horne, D. G. *Evaluated Kinetic Data for High Temperature Reactions*; Butterworths: London, 1973; p 453.

(12) An exponential smoothing function was selected on the empirical grounds that it qualitatively reproduced the $x(T)$ behavior.

(13) The reaction OH + CO also has a curved Arrhenius plot. This behavior has been explained assuming a stable HOCO intermediate using models with $V_1 > V_2$ which do not involve tunneling; see, e.g.: Mozurkewich, M.; Lamb, J. J.; Benson, S. W. *J. Phys. Chem.* **1984**, *88*, 6435, and Brunning, J.; Derbyshire, W. D.; Smith, I. W. M.; Williams, M. D. *J. Chem. Soc., Faraday Trans. 2* **1988**, *84*, 105. BAC-MP4 calculations (ref 14) support those barrier assignments. The models employed for OH + CO do not apply to reactions 1 and 2 because $V_2 > V_1$.

(14) Melius, C. F., private communication.

TABLE I: Summary of Rate Coefficient Measurements on H + N_2O

$T \pm \sigma_T$, K	P,[a] Torr	[M], 10^{18} cm^{-3}	$[N_2O]_{max}$, 10^{15} cm^{-3}	$[NH_3]$, 10^{15} cm^{-3}	$\bar{v}$, cm s^{-1}	z, cm	F, J	$k \pm \sigma_k$, cm^3 molecule^{-1} s^{-1}
414 ± 8	320	7.3	68	2.0	3.9	47[b]	17	1.8 ± 0.3 (−16)[c]
421 ± 8	220	5.0	94	3.7	7.4	47	17	2.0 ± 0.1 (−16)
422 ± 8	100	2.2	76	1.6	4.2	47	17	1.2 ± 0.2 (−16)
423 ± 8	220	4.9	87	5.0	3.4	47	29	1.8 ± 0.2 (−16)
423 ± 8	220	4.9	87	5.0	3.4	47	11	1.9 ± 0.2 (−16)
437 ± 9	380	8.2	100	5.2	6.2	47	50	2.4 ± 0.1 (−16)
442 ± 9	200	4.3	92	4.9	4.9	47	50	2.9 ± 0.4 (−16)
473 ± 9	170	3.4	68	2.4	9.1	47	17	3.2 ± 0.3 (−16)
475 ± 10	200	3.9	98	2.6	7.9	20	11	3.8 ± 0.2 (−16)
475 ± 10	200	3.9	98	2.6	7.9	20	25	3.7 ± 0.2 (−16)
476 ± 10	320	6.5	58	2.5	9.5	47	17	3.2 ± 0.4 (−16)
478 ± 10	90	1.8	57	2.6	8.9	47	17	3.3 ± 0.4 (−16)
478 ± 10	90	1.8	75	6.2	8.8	47	11	3.9 ± 0.3 (−16)
478 ± 10	90	1.8	75	6.2	8.8	47	25	3.3 ± 0.2 (−16)
482 ± 10	200	3.9	132	1.2	8.1	20	17	2.8 ± 0.3 (−16)
483 ± 10	95	1.9	75	2.8	8.7	20	17	3.3 ± 0.3 (−16)
484 ± 10	200	3.9	106	2.5	8.0	20	17	3.9 ± 0.2 (−16)
512 ± 10	120	2.2	52	6.3	10	47	25	6.2 ± 0.3 (−16)
543 ± 11	310	5.4	48	5.5	11	21	25	9.1 ± 0.6 (−16)
546 ± 11	290	5.1	72	3.2	6.1	16	25	8.6 ± 0.6 (−16)
558 ± 11	380	6.5	51	4.4	7.9	47	50	1.17 ± 0.02 (−16)
599 ± 12	120	1.9	27	5.4	12	21	11	1.2 ± 0.1 (−15)
599 ± 12	120	1.9	27	5.4	12	21	29	1.4 ± 0.1 (−15)
614 ± 12	120	1.9	33	2.0	12	47	17	1.3 ± 0.1 (−15)
615 ± 12	480	7.5	32	2.0	13	47	17	1.8 ± 0.1 (−15)
617 ± 12	200	3.2	28	2.3	12	47	11	1.6 ± 0.1 (−15)
617 ± 12	200	3.2	28	2.3	12	47	29	1.7 ± 0.1 (−15)
620 ± 12	140	2.2	35	4.0	6.3	47	17	1.4 ± 0.1 (−15)
624 ± 12	400	6.1	35	2.9	6.4	47	17	1.8 ± 0.1 (−15)
666 ± 13	220	3.1	11	3.5	9.2	15	35	3.4 ± 0.3 (−15)
700 ± 14	150	2.0	29	2.9	16	14	17	4.3 ± 0.1 (−15)
735 ± 15	300	3.4	7.9	2.1	15	15	35	4.0 ± 0.2 (−15)
762 ± 15	160	2.0	8.1	3.0	15	21	17	8.3 ± 0.2 (−15)
766 ± 15	150	1.8	16	2.5	17	14	17	7.8 ± 0.4 (−15)
769 ± 15	380	4.7	14	8.2	9.2	13	11	7.9 ± 0.5 (−15)
769 ± 15	380	4.7	14	8.2	9.2	13	29	8.2 ± 0.5 (−15)
770 ± 15	160	2.0	17	3.1	15	47	17	7.2 ± 0.3 (−15)
822 ± 16	250	2.9	4.5	0.88	22	14	17	1.00 ± 0.04 (−14)
832 ± 17	140	1.7	6.3	2.4	19	14	17	1.74 ± 0.01 (−14)
854 ± 17	200	2.3	6.0	3.6	9.5	8.3	25	2.0 ± 0.1 (−14)
894 ± 18	200	2.2	8.8	1.4	9.9	5.0	25	2.5 ± 0.1 (−14)
903 ± 18	300	3.2	7.0	4.6	10	5.0	25	4.2 ± 0.5 (−14)
920 ± 18	100	1.1	3.5	1.9	21	5.0	11	5.4 ± 0.6 (−14)
920 ± 18	100	1.1	3.5	1.9	21	5.0	29	6.0 ± 0.6 (−14)
945 ± 19	200	2.1	4.0	3.1	10	5.0	25	6.3 ± 0.4 (−14)
960 ± 19	230	2.3	5.6	4.6	15	6.0	25	8.0 ± 0.6 (−14)
1095 ± 22	200	1.8	7.2	4.2	12	4.0	25	1.5 ± 0.2 (−13)
1098 ± 22	310	2.7	11	2.8	7.9	4.0	25	1.6 ± 0.1 (−13)
1103 ± 22	230	2.0	4.6	1.4	17	6.0	25	1.7 ± 0.2 (−13)
1103 ± 22	110	0.94	5.5	3.0	18	4.0	25	1.8 ± 0.2 (−13)
1203 ± 24	180	1.5	2.5	1.2	15	3.0	25	2.9 ± 0.3 (−13)
1217 ± 24	93	0.73	2.9	1.3	30	4.0	25	4.3 ± 0.7 (−13)
1227 ± 25	55	0.43	1.5	1.3	50	3.0	25	5.2 ± 0.8 (−13)

[a] 1 Torr = 133.3 Pa. [b] z = 47 cm corresponds to premixing of the reactant and bath gases: the cooled inlet was not used. [c] Should be read as (1.8 ± 0.3) × 10^{-16}.

where HNNO*(E) denotes HNNO excited by an energy E relative to the reactants. The potential stabilization of the intermediate

$$\text{HNNO}^* + \text{M} \xrightarrow{\beta k_a} \text{HNNO} + \text{M} \qquad (9)$$

is discussed in section 4.2. Similar relations apply for the D reaction. Overall rate coefficients can be derived in a way similar to that applied to chemical activation mechanisms:[15a]

$$k_1 = \frac{1}{[\text{H}][\text{N}_2\text{O}]} \int_{V_1}^{\infty} k_b(E)\,[\text{HNNO}^*(E)]\,dE \qquad (10)$$

Any dependence of the rate coefficients on angular momentum is neglected.[16] Systems at $V_1 < E < V_2$ can only react by tunneling. Tunneling through the first barrier at TS1, Figure 3, which controls the rate of formation of HNNO*, is neglected because this barrier is broad. The curvature expressed as a complex frequency is 1287i cm^{-1}, in contrast to 2427i cm^{-1} at TS2. Thus only systems with $E > V_1$ can reach TS2; i.e., TS1 truncates the thermal distribution of E.

4.1. Kinetic Isotope Effect. We will first apply classical transition-state theory (CTST)[17] and show that it cannot explain the observations, and then show that tunneling can. According to CTST, the kinetics of OH formation will be controlled by the second, higher barrier at TS2 (Figure 3), and any earlier wells

(15) Robinson, P. J.; Holbrook, K. A. *Unimolecular Reactions*; Wiley-Interscience: London, 1972; (a) Chapter 8; (b) p 90; (c) p 144.

(16) The rotational partition functions of TS1 and TS2 are similar to that of the stable intermediate: the values relative to HNNO are 0.92 and 1.24, respectively (ref 1). According to ref 15b any centrifugal correction factors are therefore close to unity.

(17) Laidler, K. J. *Theories of Chemical Reaction Rates*; McGraw-Hill: New York, 1969; Chapters 3 and 4.

TABLE II: Summary of Rate Coefficient Measurements on D + N_2O

$T \pm \sigma_T$, K	P,[a] Torr	[M], 10^{18} cm^{-3}	$[N_2O]_{max}$, 10^{15} cm^{-3}	$[ND_3]$, 10^{15} cm^{-3}	$\bar{v}$, cm s^{-1}	z, cm	F, J	$k \pm \sigma_k$, cm^3 molecule^{-1} s^{-1}
452 ± 9	160	3.4	120	4.2	6.6	47[b]	17	1.17 ± 0.08 (−16)[c]
453 ± 9	110	2.3	100	6.0	10	47	17	1.2 ± 0.2 (−16)
459 ± 9	220	4.5	130	4.2	4.9	47	50	1.1 ± 0.1 (−16)
471 ± 9	220	4.6	110	4.4	4.8	47	25	2.0 ± 0.3 (−16)
472 ± 10	220	4.5	130	4.3	5.1	47	50	1.9 ± 0.2 (−16)
496 ± 10	410	8.0	120	4.8	5.2	47	35	2.3 ± 0.2 (−16)
516 ± 10	400	7.4	96	5.2	11	47	25	3.5 ± 0.4 (−16)
526 ± 11	110	1.9	74	5.1	12	47	25	3.71 ± 0.06 (−16)
540 ± 11	400	7.1	44	3.1	3.2	21	11	4.1 ± 0.8 (−16)
542 ± 11	390	6.9	94	3.2	3.2	21	29	4.7 ± 0.5 (−16)
563 ± 11	230	5.0	82	3.3	6.4	47	50	6.5 ± 0.8 (−16)
585 ± 12	410	6.6	54	4.3	12	21	25	8.0 ± 0.2 (−16)
588 ± 12	98	1.6	38	4.2	14	21	25	8.1 ± 0.2 (−16)
606 ± 12	110	1.6	47	4.7	13	21	25	1.08 ± 0.02 (−15)
608 ± 12	220	3.5	56	2.7	6.5	15	25	1.14 ± 0.04 (−15)
609 ± 12	100	1.6	24	1.3	14	21	25	1.28 ± 0.07 (−15)
619 ± 12	390	6.0	40	3.2	3.5	21	11	1.3 ± 0.2 (−15)
626 ± 13	370	5.6	38	1.8	11	21	11	1.7 ± 0.2 (−15)
626 ± 13	370	5.6	38	1.8	11	21	29	1.67 ± 0.09 (−15)
640 ± 13	410	6.2	19	4.2	13	21	17	1.6 ± 0.1 (−15)
642 ± 13	97	1.4	21	4.0	15	21	17	1.6 ± 0.2 (−15)
672 ± 13	220	3.1	38	2.3	7.1	15	25	2.34 ± 0.08 (−15)
698 ± 14	330	4.6	12	6.4	12	9.5	50	2.0 ± 0.2 (−15)
705 ± 14	210	2.9	11	5.6	12	8.5	35	2.4 ± 0.5 (−15)
710 ± 14	400	5.4	52	3.3	7.9	21	25	3.6 ± 0.3 (−15)
719 ± 14	86	1.1	14	5.5	11	8.5	14	3.7 ± 0.2 (−15)
733 ± 15	520	6.8	16	3.1	7.9	15	25	5.1 ± 0.6 (−15)
761 ± 15	410	5.3	6.0	3.4	16	10	17	5.1 ± 0.3 (−15)
784 ± 16	230	6.5	1.7	2.8	11	18	44	6.9 ± 0.3 (−15)
784 ± 16	120	1.4	5.9	1.4	15	12	25	8.8 ± 0.6 (−15)
792 ± 16	230	6.4	1.6	2.8	11	9.0	44	6.8 ± 0.4 (−15)
797 ± 16	230	6.4	1.7	2.8	11	9.0	11	7.9 ± 0.5 (−15)
834 ± 17	410	4.7	6.1	1.3	18	15	11	8.4 ± 0.6 (−15)
834 ± 17	410	4.7	6.1	1.3	18	15	29	8.7 ± 0.5 (−15)
835 ± 17	97	1.1	5.7	1.4	19	15	25	1.34 ± 0.02 (−14)
844 ± 17	510	5.8	4.5	1.8	13	21	25	9.7 ± 0.9 (−15)
857 ± 17	160	1.8	6.1	2.1	12	21	25	1.7 ± 0.1 (−14)
869 ± 17	77	0.9	3.8	1.3	37	18	17	2.1 ± 0.2 (−14)
883 ± 18	170	1.9	5.9	4.8	33	18	17	3.7 ± 0.3 (−14)
933 ± 19	54	0.6	4.7	3.5	26	10	35	7.8 ± 0.7 (−14)
945 ± 19	300	3.1	3.0	1.4	20	15	17	3.1 ± 0.1 (−14)
945 ± 19	110	1.1	3.2	1.4	20	15	11	5.79 ± 0.09 (−14)
945 ± 19	110	1.1	3.2	1.4	20	15	29	5.8 ± 0.1 (−14)
959 ± 19	230	2.3	2.8	7.8	14	4.5	25	3.8 ± 0.6 (−14)
964 ± 19	240	2.4	3.0	1.3	14	4.5	44	5.1 ± 0.2 (−14)
968 ± 19	160	1.6	5.1	7.9	21	18	17	5.7 ± 0.4 (−14)
1009 ± 20	140	1.3	3.3	0.52	26	7.0	25	6.9 ± 0.3 (−14)
1022 ± 20	560	5.3	7.3	4.7	11	7.0	11	1.0 ± 0.1 (−13)
1111 ± 22	470	4.0	6.9	3.7	15	8.0	25	1.31 ± 0.04 (−13)
1120 ± 22	78	0.70	2.4	0.72	32	2.5	17	2.0 ± 0.1 (−13)
1129 ± 23	160	1.4	4.4	2.6	16	4.0	25	2.33 ± 0.06 (−13)
1149 ± 23	470	3.9	7.0	3.5	16	8.0	29	1.29 ± 0.08 (−13)
1165 ± 23	470	3.9	5.2	3.7	16	10	25	1.1 ± 0.1 (−13)
1210 ± 24	78	0.65	1.6	0.72	34	2.5	21	2.6 ± 0.4 (−13)

[a] 1 Torr = 133.3 Pa. [b] z = 47 cm corresponds to premixing of the reactant and bath gases: the cooled inlet was not used. [c] Should be read as (1.17 ± 0.08) × 10^{-16}.

or lower barriers are irrelevant. Under those circumstances $k_1(T)$ could be written in a canonical form

$$k_1(T) = (k_B T/h) Q_{TS2}/[Q_H Q_{N_2O}] \exp(-V_2/RT) \quad (11)$$

An analogous expression can be written for k_2, so that the CTST estimate for the kinetic isotope effect is

$$x(T) = (Q_{TS2,H}/Q_{TS2,D})(Q_D/Q_H) \exp\{(V_{2,D} - V_{2,H})/RT\} \quad (12)$$

These CTST values of x, calculated with the data given in the Appendix, are compared in Figure 2 to the experimental data. Calculated values are in accord with observation for $T > 900$ K. Equation 12 is clearly inadequate at lower temperatures, where the lower zero-point energy of TS2 for D, with respect to TS2 for H, i.e., $V_{2,D} < V_{2,H}$, overcomes the lower collision rate for D atoms and CTST predicts $k_1 < k_2$.

The validity of this argument is independent of the selected properties of the transition state, because the zero-point energy of the reactants is unchanged upon substitution of D for H, while the vibrational frequencies of *any* activated complex will be lowered. For example, an $NNOH^{\ddagger}$ activated complex can be considered in the context of direct attack by H at the oxygen end of N_2O.[1] Figure 2 shows that eq 12 applied to this complex conflicts as well with experiment. In section 4.2 we will show that the temperature dependence of $x(T)$ predicted for the potential recombination channel, eq 9, also disagrees with the experimental results.

Thus, another factor, not considered in CTST, keeps $k_1 > k_2$ at all temperatures and increases in significance at lower temperatures. The influence of tunneling would be to increase k_1 more than k_2 at any given temperature because the larger de Broglie wavelength of H as compared to D permits greater penetration of a barrier. As T is reduced the classical reaction ($E > V_2$) is reduced and quantum effects dominate. Therefore tunneling would lead to an increasing kinetic isotope effect as the temperature is

reduced, in accord with our findings, Figure 2.

4.2. Pressure Independence of the Rate Coefficients. $k_{-a}(E)$ and $k_b(E)$ in eq 8 may be calculated by using RRKM theory. Our input data and modifications to the usual RRKM approach to incorporate tunneling are given in the Appendix. We calculate that, at, for example, only 2 kJ mol^{-1}, an energy smaller than RT, above the threshold V_1, $k_{-a} = 1 \times 10^{10}$ s^{-1} and $k_b = 2 \times 10^8$ s^{-1}. Fragmentation of HNNO* is therefore faster than stabilization (eq 9), assuming $\beta k_s = 2 \times 10^{-10}$ cm^3 s^{-1},[1] at the experimental [M] employed ($\lesssim 10^{19}$ cm^{-3}, see Tables I and II). k_{-a} and k_b increase with E; thus quenching should have a negligible effect on the distribution of HNNO*(E) and hence k_1, which explains our observed pressure independence. This treatment is consistent with the earlier conclusion, derived from QRRK[18] estimates, that any recombination of H and N_2O would be in the low-pressure third-order limit under the HTP conditions.[1] Similar QRRK calculations now made for the D analogues indicate that D recombination with N_2O would also be third order.

The kinetic isotope effect for the potential recombination channel can now be derived from these QRRK results. Using input data from the Appendix and the earlier study,[1] we find, for a midrange value of [M] = 5×10^{18} cm^{-3} at 450 and 1000 K, $x = 0.68$ and $x = 0.72$, respectively. Again, these values disagree with experiment. The values of x below unity are as expected because DNNO has a greater density of states than HNNO. Together with the observed pressure independence of reactions 1 and 2, $x(T)$ is further evidence against the dominance of an addition channel at low temperatures.

5. Conclusion

Our results point qualitatively to a significant role for tunneling in the rate-controlling step. This mechanism not only explains the curvature in the Arrhenius plots of $k_1(T)$ and $k_2(T)$, but also the temperature dependence of the kinetic isotope effect which is inconsistent with CTST alone. Major loss of H or D by recombination with N_2O is ruled out both by the kinetic isotope effect and by the lack of observed pressure dependence. A more rigorous theoretical investigation of reactions 1 and 2, which incorporates variational transition-state theory and multidimensional tunneling on a full potential energy surface, is under way elsewhere.[19]

Acknowledgment. This work was supported by the U.S. Army Research Office. We are grateful to W. F. Flaherty and D. J. Rovero for technical assistance and to Dr. C. F. Melius (Sandia National Laboratories) for allowing us to quote unpublished results. We thank him and Dr. B. C. Garrett (Chemical Dynamics Corp.) for helpful discussions.

Appendix

The structures of the transition states and intermediate complexes for reactions 1 and 2, as well as the vibrational frequencies for reaction 1, derived from BAC-MP4 calculations, have been given previously.[1] The BAC-MP4 method involves ab initio quantum calculations to identify the geometries and vibrational frequencies at the stationary points, i.e., transition states and stable intermediates, of the potential energy surface at the Hartree–Fock level. The energies of the stationary points are calculated by using Møller–Plesset fourth-order perturbation theory followed by semiempirical bond additivity corrections.[1] Here we give the vibrational frequencies for reaction 2 calculated by C. F. Melius[14] (species, vibrational frequencies, cm^{-1}): DNNO‡(TS1), 999*i*, 307, 573, 651, 1162, 1816; ^{2}A′ *cis*-DNNO, 300, 704, 956, 1085, 1428, 2346; $\overline{\text{DNNO}}^‡$(TS2), 1767*i*, 480, 735, 801, 1255, 1301. Melius has made new energy calculations, on both reactions 1 and 2, which incorporate slightly modified spin corrections.[14] Energies for the vibrationally adiabatic ground-state PES, relative to the reactants and using the labeling of Figure 3, are as follows. H + N_2O: $V_1 = 38.6$, $V_2 = 63.4$, $V_3 = -61.2$ kJ mol^{-1}. D + N_2O: $V_1 = 37.1$, $V_2 = 58.6$, $V_3 = -70.2$ kJ mol^{-1}.

We employ these BAC-MP4 data to make RRKM calculations, which include tunneling, as outlined by Miller[20] and Forst.[21] The energy-dependent fragmentation rate coefficient $k(E)$ for an excited molecule is

$$k(E) = W^‡(E)/\{hN(E)\} \tag{13}$$

$N(E)$ is the density of states of the molecule, here calculated under the harmonic oscillator approximation by the method of steepest descents.[15c] $W^‡(E)$ is the integrated density of states of the transition state, which in its generalized form is given by[21]

$$W^‡(E) = \int_0^E p(u)\, N^‡(E-u)\, du \tag{14}$$

where $p(u)$ is the transmission probability at energy u. We calculate $p(u)$ by fitting an Eckart potential[22] to the PES. To avoid a subtraction catastrophe as $p(u) \to 0$ we rewrite Brown's expression for an exoergic reaction[23] as

$$p(u) = \frac{2 \sinh(a) \sinh(b)}{\cosh(a+b) + \cosh(d)} \tag{15}$$

With U_1 and U_2 as the heights of each side of an asymmetrical Eckart barrier and ν^* as the conjugate of the complex frequency at its peak,

$$a = \pi\{u/c\}^{1/2} \tag{16}$$

$$b = \pi\{(u - U_1 + U_2)/c\}^{1/2} \tag{17}$$

$$c = \{h\nu^*(U_1^{-1/2} + U_2^{-1/2})/4\}^2 \tag{18}$$

$$d = \pi\{(U_1^{1/2} + U_2^{1/2})^2/c - 1\}^{1/2} \tag{19}$$

If d is complex then cos (id) should be substituted for cosh (d) in eq 15.

Registry No. H, 12385-13-6; D, 16873-17-9; N_2O, 10024-97-2; NH_3, 7664-41-7; ND_3, 13550-49-7.

(18) Dean, A. M. *J. Phys. Chem.* **1985**, *89*, 4600.
(19) Garrett, B. C.; Melius, C. F., private communication.
(20) Miller, W. H. *J. Am. Chem. Soc.* **1979**, *101*, 6810.
(21) Forst, W. *J. Phys. Chem.* **1983**, *87*, 4489.
(22) Johnston, H. S. *Gas Phase Reaction Rate Theory*; Ronald: New York, 1966; Chapter 2.
(23) Brown, R. L. *J. Res. Natl. Bur. Stand.* **1981**, *86*, 605.